Weighted Poisson–Delaunay Mosaics*

Herbert Edelsbrunner[1] and Anton Nikitenko[1]

1 **IST Austria (Institute of Science and Technology Austria), Am Campus 1, 3400 Klosterneuburg, Austria,** edels@ist.ac.at, anton.nikitenko@ist.ac.at

Abstract

Slicing a Voronoi tessellation in $\mathbb{R}^n$ with a k-plane gives a k-dimensional weighted Voronoi tessellation, also known as power diagram or Laguerre tessellation. Mapping every simplex of the dual weighted Delaunay mosaic to the radius of the smallest empty circumscribed sphere whose center lies in the k-plane gives a generalized discrete Morse function. Assuming the Voronoi tessellation is generated by a Poisson point process in $\mathbb{R}^n$, we study the expected number of simplices in the k-dimensional weighted Delaunay mosaic as well as the expected number of intervals of the Morse function, both as functions of a radius threshold. As a byproduct we obtain a new proof for the expected number of connected components (*clumps*) in a line section of a circular Boolean model in $\mathbb{R}^n$.

1998 ACM Subject Classification: I.3.5 Computational Geometry and Object Modeling, G.3 Probability and Statistics, G.2 Discrete Mathematics.

2010 AMS Mathematics Subject Classification: 60D05 Geometric probability and stochastic geometry, 68U05 Computer graphics; computational geometry.

Keywords and phrases: Voronoi tessellations, Laguerre distance, weighted Delaunay mosaics; discrete Morse theory, critical simplices, intervals; stochastic geometry, Poisson point process, Boolean model, clumps; Slivnyak–Mecke formula, Blaschke–Petkantschin formula.

1 Introduction

Given a discrete set of points $Y \subseteq \mathbb{R}^k$, the *Voronoi tessellation* tiles the k-dimensional Euclidean space with convex polyhedra, each consisting of all points $a \in \mathbb{R}^k$ for which a particular point y is closest among all points in Y. To generalize, suppose each $y \in Y$ has a weight $w \in \mathbb{R}$, and substitute the *power distance* of a from y, defined as $\|a - y\|^2 - w$, for the squared Euclidean distance in the definition of the Voronoi tessellation. The resulting tiling of $\mathbb{R}^k$ into convex polyhedra is known by several names, including *power diagrams* [1] and *Laguerre tessellations* [14], but to streamline language we will call them *weighted Voronoi tessellations*. They do indeed look like unweighted Voronoi tessellations, except that the hyperplane separating two neighboring polyhedra does not necessarily lie halfway between the generating points; see Figure 1. Our motivation for studying weighted Voronoi tessellations derives from the extra degree of freedom — the weight — which permits better approximations of observed tilings, such as cell cultures in plants [21] and microstructures of materials [4]. Beyond this practical consideration, there is an intriguing connection between the volumes of skeleta of unweighted Voronoi tessellations and the number of simplices in weighted Delaunay mosaics through the Crofton's formula, which is worth exploring.

Our preferred construction takes a k-dimensional slice through a Voronoi tessellation in $\mathbb{R}^n$; see [2, 23]. Specifically, if X is a discrete set of points in $\mathbb{R}^n$ and $\mathbb{R}^k \hookrightarrow \mathbb{R}^n$ is spanned

* This work is partially supported by the Austrian Science Fund (FWF), grant no. I02979-N35.

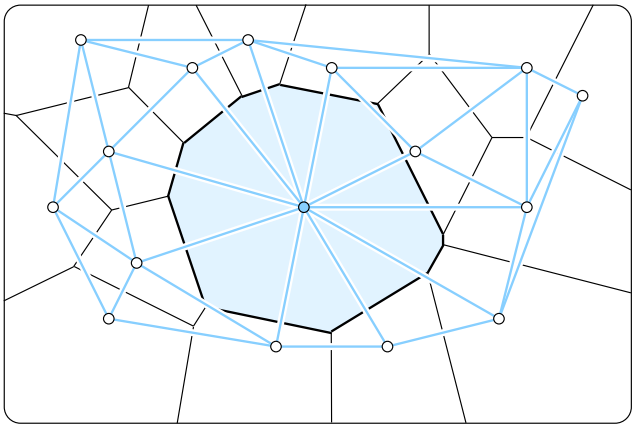

Figure 1 Weighted Voronoi tessellation in $\mathbb{R}^2$ with superimposed weighted Delaunay mosaic. All points have zero weight except the point with the shaded domain, which has positive weight.

by the first $k \leq n$ coordinate axes, then the Voronoi tessellation of X in $\mathbb{R}^n$ intersects $\mathbb{R}^k$ in a k-dimensional weighted Voronoi tessellation. The points in $\mathbb{R}^k$ that generate the weighted tessellation are the orthogonal projections y_x of the points $x \in X$, and their weights are $w_x = -\|x - y_x\|^2$. While all weights in this construction are non-positive, this is not a restriction of generality because the tessellation remains unchanged when all weights are increased by the same amount. Indeed, every weighted Voronoi tessellation with bounded weights can be obtained as a slice of an unweighted Voronoi tessellation. It is often more convenient to consider the dual of a weighted Voronoi tessellation, which is again known by several names, including *Laguerre triangulation* [19] and *regular triangulation* [9], but we will call them *weighted Delaunay mosaics*. An important difference to the unweighted concept is that the Voronoi polyhedron of a weighted point may be empty, in which case this weighted point will not be a vertex of the weighted Delaunay mosaic. For generic sets of weighted points, the weighted Delaunay mosaic is a simplicial complex in $\mathbb{R}^k$. Since we focus on slices of unweighted Voronoi tessellations, we define the general position only in this case. Specifically, we say a discrete set $X \subseteq \mathbb{R}^n$ is *generic* if the following conditions are satisfied for every $0 \leq j < n$:

1. no $j + 2$ points belong to a common j-plane,
2. no $j + 3$ points belong to a common j-sphere,
3. considering the unique j-sphere that passes through $j + 2$ points, no $j + 1$ of these points belong to a j-plane that passes through the center of the j-sphere,
4. considering the unique j-plane that passes through $j + 1$ points, this plane is neither orthogonal nor parallel to $\mathbb{R}^k$,
5. no two points have identical distance to $\mathbb{R}^k$.

For $j = 0$, property 4 means that no point of X is in $\mathbb{R}^k$. We note that the Poisson point process is generic with probability 1.

Continuing the work started in [7], we are interested in the stochastic properties of the weighted Delaunay mosaics and their radius functions. To explain the latter concept, we assume the generic case in which the mosaic is a simplicial complex, and for every simplex $Q' \in \operatorname{Del} Y$ with preimage $Q \subseteq \mathbb{R}^n$, we find the smallest $(n-1)$-sphere that satisfies the following properties:

- it passes through all vertices of Q (it is a *circumscribed sphere* of Q),

- the open ball it bounds does not contain any points of X (it is *empty*),
- its center lies in $\mathbb{R}^k$ (it is *anchored*).

The existence of such spheres for the simplices of the weighted mosaic can be shown in a way similar to the unweighted case [5] and is left to the reader. We call this sphere the *circumsphere* and its radius the *radius* of $Q' \in \operatorname{Del} Y$. Similarly, we call the sphere the *anchored circumsphere* and its center the *anchor* of Q. The *radius function* of the weighted Delaunay mosaic, $\mathcal{R}\colon \operatorname{Del} Y \to \mathbb{R}$, maps every simplex to its radius. It partitions $\operatorname{Del} Y$ into *intervals* of simplices that share the same sphere and therefore the same function value. These intervals have topological significance [8]: adding the simplices in the order of increasing radius, the homotopy type of the complex changes whenever the interval contains a single simplex and it remains unchanged whenever the interval contains two or more simplices. Indeed, the operation in the latter case is known as anticollapse and has been studied extensively in combinatorial topology. Each interval is defined by two simplices $L \subseteq U$ in the weighted Delaunay mosaic and consists of all simplices that contain L and are contained in U. We call $Q' \in \operatorname{Del} Y$ a *critical simplex* of $\mathcal{R}$ if it is the sole simplex in its interval: $L = Q' = U$, and we call Q' a *regular simplex* of $\mathcal{R}$, otherwise. The *type* of the interval is the pair of dimensions of the lower and the upper bound: (ℓ, m) in which $\ell = \dim L$ and $m = \dim U$. Our main result is an extension of the stochastic findings about the radius function of the Poisson–Delaunay mosaic in [7] from the unweighted to the weighted case.

▶ **Theorem 1** (Main Result). *Let X be a Poisson point process with density in $\mathbb{R}^n$ and $\mathbb{R}^k \hookrightarrow \mathbb{R}^n$. There are constants $C^{k,n}_{\ell,m}$ such that for any $r_0 \geq 0$, the expected number of intervals of type (ℓ, m) in the k-dimensional weighted Poisson–Delaunay mosaic with center in a Borel set $\Omega \subseteq \mathbb{R}^k$ and radius at most r_0 is*

$$\mathbb{E}[c^{k,n}_{\ell,m}(r_0)] = C^{k,n}_{\ell,m} \cdot \frac{\gamma\big(m+1-\frac{k}{n};\, \rho\nu_n r_0^n\big)}{\Gamma\big(m+1-\frac{k}{n}\big)} \cdot \rho^{\frac{k}{n}} \|\Omega\|, \tag{1}$$

in which ν_n is the volume of the unit ball in $\mathbb{R}^n$, and we give explicit computations of the constants in $k \leq 2$ dimensions. Similarly, the expected number of j-dimensional simplices in the weighted Poisson–Delaunay mosaic with center in a Borel set $\Omega \subseteq \mathbb{R}^k$ and radius at most r_0 is:

$$\mathbb{E}[d^{k,n}_j(r_0)] = \left[\sum_{m=j}^{k} \frac{\gamma\big(m+1-\frac{k}{n};\, \rho\nu_n r_0^n\big)}{\Gamma\big(m+1-\frac{k}{n}\big)} \sum_{\ell=0}^{j} \binom{m-\ell}{m-j} C^{k,n}_{\ell,m}\right] \cdot \rho^{\frac{k}{n}} \|\Omega\|. \tag{2}$$

In an equivalent formulation, this theorem states that the radius of a *typical interval* is Gamma-distributed, whereas the radius of a *typical simplex* is a mixture of Gamma distributions; compare with [7]. In a more general context, the contributions of this paper are to the field of stochastic geometry, which was summarized in the text by Schneider and Weil [22]. The particular questions on Poisson–Delaunay mosaics studied in this paper have been pioneered by Miles almost 50 years ago [16, 17]. Formulas for the weighted case have also been derived by Møller [18], but these are restricted to top-dimensional simplices whose expected numbers can be derived using Crofton's formula and expected volumes of Voronoi skeleta.

Outline. Section 2 discusses the case $k = 1$ as a warm-up exercise. It is sufficiently elementary so that explicit formulas can be derived without reliance on more difficult to prove general integral formulas. We also show how to get the expected number of connected components in the intersection of a line with a circular Boolean model in $\mathbb{R}^n$ using discrete

Morse theory in this section. Section 3 proves a Blaschke–Petkantschin type formula for the general weighted case. Section 4 uses this formula to prove our main result. Section 5 develops explicit expressions for all types of intervals in two dimensions. Section 6 concludes this paper. Appendix A introduces the special functions and distributions used in the derivation of our results.

2 One Dimension

In $k = 1$ dimension, the weighted Delaunay mosaic has a simple structure so that results can be obtained by elementary means.

Slice construction. Let $n \geq 2$ and let $X \subseteq \mathbb{R}^n$ be a stationary Poisson point process with density $\rho > 0$. We write $\mathbb{R}^1 \hookrightarrow \mathbb{R}^n$ for the first coordinate axis, which is a directed line passing through $\mathbb{R}^n$. For each point $x = (x_1, x_2, \ldots, x_n) \in X$, we write $y_x = (x_1, 0, \ldots, 0)$ for the projection onto $\mathbb{R}^1$ and $-w_x = x_2^2 + x_3^2 + \ldots + x_n^2$ for its squared distance from the line. Letting $Y = \{(y_x, w_x) \mid x \in X\}$ be the resulting set of weighted points in $\mathbb{R}^1$, we are interested in its weighted Voronoi tessellation, $\operatorname{Vor} Y$, and its weighted Delaunay mosaic, $\operatorname{Del} Y$. By construction, the former is the intersection of the n-dimensional (unweighted) Voronoi tessellation with the line: $\operatorname{Vor} Y = \{\operatorname{domain}(x) \cap \mathbb{R}^1 \mid x \in X\}$. As discussed above, the interval $\operatorname{domain}(x) \cap \mathbb{R}^1$ belongs to the weighted Voronoi tessellation iff there is an anchored circumsphere of x, that is: an empty sphere centered in $\mathbb{R}^1$ that passes through x. Similarly, two weighted Voronoi domains, $\operatorname{domain}(x) \cap \mathbb{R}^1$ and $\operatorname{domain}(u) \cap \mathbb{R}^1$, share an endpoint iff there is an empty anchored sphere passing through x and u. It follows that every edge in $\operatorname{Del} Y$ is the projection of an edge in $\operatorname{Del} X$; see Figure 2. As suggested

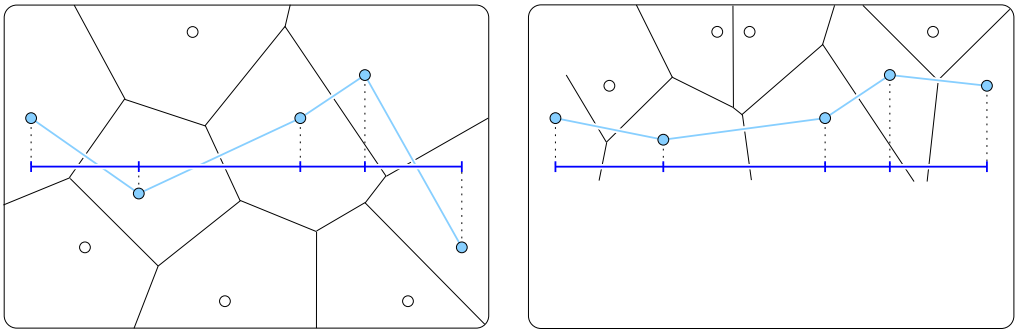

Figure 2 *Left:* a 1-dimensional weighted Voronoi tessellation as a slice of a 2-dimensional unweighted Voronoi tessellation. The weighted Delaunay mosaic in $\mathbb{R}^1$ is the projection of a chain of edges in the 2-dimensional unweighted Delaunay mosaic. *Right:* reflecting the points across $\mathbb{R}^1$ affects the 2-dimensional Voronoi tessellation but not the 1-dimensional slice.

in this figure, we can simplify the construction by reducing n to 2. Writing $\mathbf{H}$ for the half-plane of points whose first coordinate is arbitrary, whose second coordinate is non-negative, and whose remaining $n - 2$ coordinates vanish, we map $x = (x_1, x_2, \ldots, x_n) \in \mathbb{R}^n$ to $x' = (x_1, \sum_{i=2}^n x_i^2, 0, \ldots, 0) \in \mathbf{H}$. This amounts to rotating x about $\mathbb{R}^1$ into $\mathbf{H}$. Let X' be the resulting set of points in $\mathbf{H}$ and Y' the set of weighted points in $\mathbb{R}^1$ obtained by projection from X'. Then $Y = Y'$, which shows that X and X' define the same 1-dimensional weighted Voronoi tessellation and weighted Delaunay mosaic. There is a small price to pay for the simplification, namely that the projected Poisson point process in $\mathbf{H}$ is not necessarily homogeneous. Specifically, the projected process in $\mathbf{H}$ is a Poisson point process

with *intensity* $\varrho(x) = \sigma_{n-1}\rho x_2^{n-2}$, in which σ_{n-1} is the $(n-2)$-dimensional volume of the unit sphere in $\mathbb{R}^{n-1}$.

Interval structure. We now return to the intervals of the radius function in one dimension, $\mathcal{R}\colon \operatorname{Del} Y \to \mathbb{R}$. In the assumed generic case, $\operatorname{Del} Y$ contains only two kinds of simplices: vertices and edges. By definition, the value of $\mathcal{R}$ at a simplex $Q' \in \operatorname{Del} Y$ is the radius of the anchored circumsphere of the preimage of Q'. There are only three types of intervals $[L, U]$:

(0, 0): here $L = U$ and $\dim L = \dim U = 0$. The interval contains a single and therefore critical vertex.

(1, 1): here $L = U$ and $\dim L = \dim U = 1$. The interval contains a single and therefore critical edge.

(0, 1): here $L \subseteq U$ and $\dim L = \dim U - 1$. The interval is a pair consisting of a regular vertex and a regular edge. We call it a *vertex-edge pair* if the vertex precedes the edge as we go from left to right, and we call it an *edge-vertex pair*, otherwise.

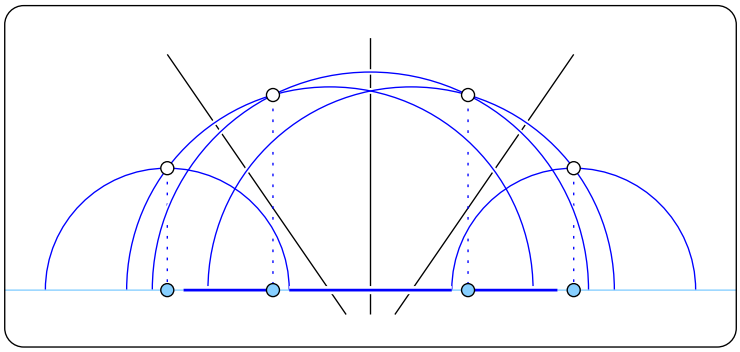

Figure 3 From *left* to *right* on the horizontal line: a critical vertex, an edge-vertex pair, a critical edge, a vertex-edge pair, and another critical vertex.

The cases can be distinguished geometrically, as illustrated in Figure 3. Let $x = (x_1, x_2) \in \mathbf{H}$ and $y_x = (x_1, 0)$ with weight $w_x = -x_2^2$. Then $L = U = \{y_x\}$ is a critical vertex of $\operatorname{Del} Y$ iff y_x is the anchor of x. Otherwise, the anchored circumcircle of x also passes through a second point, $u \in X \subseteq \mathbf{H}$, with y_x and y_u on the same side of the anchor. In this case, $L = \{y_x\}$ and $U = \{y_x, y_u\}$ form a vertex-edge or an edge-vertex pair. Finally, we have a critical edge $L = U = \{y_x, y_u\}$ if y_x and y_u lie on opposite sides of the anchor.

We will make essential use of the geometric characterization of interval types when we compute their expected numbers. To simplify the computation, we note that the structure along $\mathbb{R}^1$ is a strict repetition of the following pattern: a critical vertex, a non-negative number of edge-vertex pairs, a critical edge, and a non-negative number of vertex-edge pairs.

Critical vertices. We begin with computing the number of critical vertices, $c_{0,0}^{1,n}$, inside a region $\Omega \subseteq \mathbb{R}^1$ and with radius at most some threshold r_0. Let $x = (x_1, x_2) \in X \subseteq \mathbf{H}$ and note that the smallest anchored circle passing through x has center $y_x = (x_1, 0)$ and radius $r = x_2$. Write $\mathbb{P}_\emptyset(x)$ for the probability that this circle is empty, $\mathbf{1}_\Omega(x)$ for the indicator that $y_x \in \Omega$, and $\mathbf{1}_{r_0}(x)$ for the indicator that $r \leq r_0$. We use the Slivnyak–Mecke formula to compute

$$\mathbb{E}[c_{0,0}^{1,n}(r_0)] = \int_{x \in \mathbf{H}} \mathbf{1}_\Omega(x)\mathbf{1}_{r_0}(x)\mathbb{P}_\emptyset(x)\varrho(x)\,\mathrm{d}x; \tag{3}$$

compare with [7]. The intensity measure of the upper semi-circle with radius r is of course ρ times the volume of an n-ball with radius r, which we write as $\rho\nu_r r^n$. Hence, $\mathbb{P}_\emptyset(x) = e^{-\rho\nu_n r^n}$. In other words, the probability that the anchored circle is empty is the probability that the n-ball whose points get rotated into the semi-disk is empty. So we have

$$\mathbb{E}[c^{1,n}_{0,0}(r_0)] = \int_{x_1\in\Omega}\int_{r=0}^{r_0} e^{-\rho\nu_n r^n}\rho\sigma_{n-1}r^{n-2}\,\mathrm{d}r\,\mathrm{d}x_1 = \|\Omega\|\sigma_{n-1}\rho\int_{r=0}^{r_0} r^{n-2}e^{-\rho\nu_n r^n}\,\mathrm{d}r. \tag{4}$$

To evaluate this integral, we use the identity on Gamma functions proved as Lemma 4 in Appendix A, where the functions are defined. In this application, the integral on the right-hand side in (4) evaluates to $\gamma\big(1-\frac{1}{n};\,\rho\nu_n r_0^n\big)/[n\cdot(\rho\nu_n)^{1-\frac{1}{n}}]$. Writing $c^{1,n}_{0,0} = c^{1,n}_{0,0}(\infty)$, we set $r_0 = \infty$ to get the expected total number of critical vertices, and we write the expected number up to radius r_0 as a fraction of the former:

$$\mathbb{E}[c^{1,n}_{0,0}] = \frac{\sigma_{n-1}\Gamma\big(1-\frac{1}{n}\big)}{n\nu_n^{1-1/n}}\cdot\|\Omega\|\rho^{\frac{1}{n}}, \tag{5}$$

$$\mathbb{E}[c^{1,n}_{0,0}(r_0)] = \frac{\gamma\big(1-\frac{1}{n};\,\rho\nu_n r_0^n\big)}{\Gamma\big(1-\frac{1}{n}\big)}\cdot\mathbb{E}[c^{1,n}_{0,0}]. \tag{6}$$

Regular edges. To count the regular edges — or intervals of type $(0,1)$ — we again use the Slivnyak–Mecke formula. Let $x = (x_1, x_2)$ and $u = (u_1, u_2)$ be two points in $X \subseteq \mathbf{H}$. There is a unique anchored circle that passes through both points, and the edge connecting y_x and y_u belongs to $\operatorname{Del} Y$ iff this circle is empty. Writing $(z_1, 0)$ for the center and r for the radius, the edge is critical, if $x_1 < z_1 < u_1$, and regular, otherwise; see Figure 3. Write $\mathbb{P}_\emptyset(x,u)$ for the probability that the unique anchored circle passing through x and u is empty, $\mathbf{1}_\Omega(x,u)$ for the indicator that $z_1 \in \Omega$, write $\mathbf{1}_{r_0}(x,u)$ for the indicator that $r \le r_0$, and $\mathbf{1}_{0,1}(x,u)$ for the indicator that x_1 and u_1 lie on the same side of z_1. By Slivnyak–Mecke formula, we have

$$\mathbb{E}[c^{1,n}_{0,1}(r_0)] = \frac{1}{2!}\int_{u\in\mathbf{H}}\int_{x\in\mathbf{H}} \mathbf{1}_\Omega(x,u)\mathbf{1}_{r_0}(x,u)\mathbf{1}_{0,1}(x,u)\mathbb{P}_\emptyset(x,u)\varrho(x)\varrho(u)\,\mathrm{d}x\,\mathrm{d}u. \tag{7}$$

We already know that $\mathbb{P}_\emptyset(x,u) = e^{-\rho\nu_n r^n}$. To compute the rest, we do a change of variables, re-parametrizing the points by the center and radius of the unique anchored circle passing through them and two angles: $x = (z_1 + r\cos\xi, r\sin\xi)$ and $u = (z_1 + r\cos\upsilon, r\sin\upsilon)$, in which $0 \le \xi, \upsilon < \pi$. This is a bijection up to a set of measure 0. The Jacobian of this change of variables is the absolute determinant of the matrix of old variables derived by the new variables:

$$J = \operatorname{abs}\begin{vmatrix} 1 & \cos\xi & -r\sin\xi & 0 \\ 0 & \sin\xi & r\cos\xi & 0 \\ 1 & \cos\upsilon & 0 & -r\sin\upsilon \\ 0 & \sin\upsilon & 0 & r\cos\upsilon \end{vmatrix} = r^2|\cos\upsilon - \cos\xi|. \tag{8}$$

With the new variables, the indicators can be absorbed into integration limits: $\mathbf{1}_\Omega(x,u) = 1$ iff $z_1 \in \Omega$, and $\mathbf{1}_{0,1}(x,u) = 1$ iff ξ and υ are either both smaller or both larger than $\frac{\pi}{2}$. The two cases are symmetric, so we assume the former and multiply with 2. The integral in (7)

thus turns into

$$\mathbb{E}[c_{0,1}^{1,n}(r_0)] = \int_{z_1\in\Omega}\int_{r=0}^{r_0} e^{-\rho\nu_n r^n}\int_{0\le\xi,\upsilon<\frac{\pi}{2}} \rho^2\sigma_{n-1}^2(r^2\sin\xi\sin\upsilon)^{n-2}r^2|\cos\upsilon-\cos\xi|\,\mathrm{d}\xi\,\mathrm{d}\upsilon\,\mathrm{d}r\,\mathrm{d}z_1 \quad (9)$$

$$= \|\Omega\|\rho^2\sigma_{n-1}^2\int_{r=0}^{r_0} e^{-\rho\nu_n r^n}r^{2n-2}\,\mathrm{d}r\int_{0\le\xi,\upsilon<\frac{\pi}{2}}(\sin\xi\sin\upsilon)^{n-2}|\cos\upsilon-\cos\xi|\,\mathrm{d}\xi\,\mathrm{d}\upsilon. \quad (10)$$

We apply Lemma 4 to evaluate the integral over the radius, and we use the Mathematica software to evaluate the integral over the two angles:

$$\int_{r\le r_0} r^{2n-2}e^{-\rho\nu_n r^n}\,\mathrm{d}r = \tfrac{\gamma\left(2-\frac{1}{n};\rho\nu_n r_0^n\right)}{n(\rho\nu_n)^{2-\frac{1}{n}}}, \quad (11)$$

$$\int_{0\le\xi,\upsilon<\frac{\pi}{2}}(\sin\xi\sin\upsilon)^{n-2}|\cos\upsilon-\cos\xi|\,\mathrm{d}\xi\,\mathrm{d}\upsilon = \tfrac{\sqrt{\pi}}{n-1}\left[\tfrac{2\Gamma(n-1)}{\Gamma\left(n-\frac{1}{2}\right)}-\tfrac{\Gamma\left(\frac{n-1}{2}\right)}{\Gamma\left(\frac{n}{2}\right)}\right]. \quad (12)$$

Setting $r_0=\infty$, we get the expected total number of regular edges, and as before we write the expected number up to radius r_0 as a fraction of the total number:

$$\mathbb{E}[c_{0,1}^{1,n}] = \tfrac{\sigma_{n-1}^2\Gamma\left(2-\frac{1}{n}\right)}{n\nu_n^{2-1/n}}\tfrac{\sqrt{\pi}}{n-1}\left[\tfrac{2\Gamma(n-1)}{\Gamma\left(n-\frac{1}{2}\right)}-\tfrac{\Gamma\left(\frac{n-1}{2}\right)}{\Gamma\left(\frac{n}{2}\right)}\right]\cdot\|\Omega\|\rho^{\frac{1}{n}}, \quad (13)$$

$$\mathbb{E}[c_{0,1}^{1,n}(r_0)] = \tfrac{\gamma\left(2-\frac{1}{n};\rho\nu_n r_0^n\right)}{\Gamma\left(2-\frac{1}{n}\right)}\cdot\mathbb{E}[c_{0,1}^{1,n}]. \quad (14)$$

Summary. Recall that the critical vertices and the critical edges alternate along $\mathbb{R}^1$, which implies that their expected total number is the same. The dependence on the radius threshold, r_0, is however different. Here we notice that the dependence on the radius for $c_{1,1}^{1,n}$ is the same as for $c_{0,1}^{1,n}$ because what changes in the integration are only the admissible angles. Extracting the constants from the formulas for the expectation, we use (5) and (13) to get

$$C_{0,0}^{1,n} = C_{1,1}^{1,n} = \tfrac{\sigma_{n-1}\Gamma\left(1-\frac{1}{n}\right)}{n\nu_n^{1-1/n}}, \quad (15)$$

$$C_{0,1}^{1,n} = \tfrac{\sigma_{n-1}^2\sqrt{\pi}\Gamma\left(2-\frac{1}{n}\right)}{n(n-1)\nu_n^{2-1/n}}\left[\tfrac{2\Gamma(n-1)}{\Gamma\left(n-\frac{1}{2}\right)}-\tfrac{\Gamma\left(\frac{n-1}{2}\right)}{\Gamma\left(\frac{n}{2}\right)}\right]; \quad (16)$$

see Table 1. We write the expectations as fractions of these constants times the size of the region times the n-th root of the density in $\mathbb{R}^n$:

$$\mathbb{E}[c_{0,0}^{1,n}(r_0)] = C_{0,0}^{1,n}\cdot\tfrac{\gamma\left(1-\frac{1}{n};\rho\nu_n r_0^n\right)}{\Gamma\left(1-\frac{1}{n}\right)}\cdot\|\Omega\|\rho^{1/n}, \quad (17)$$

$$\mathbb{E}[c_{0,1}^{1,n}(r_0)] = C_{0,1}^{1,n}\cdot\tfrac{\gamma\left(2-\frac{1}{n};\rho\nu_n r_0^n\right)}{\Gamma\left(2-\frac{1}{n}\right)}\cdot\|\Omega\|\rho^{1/n}, \quad (18)$$

$$\mathbb{E}[c_{1,1}^{1,n}(r_0)] = C_{1,1}^{1,n}\cdot\tfrac{\gamma\left(2-\frac{1}{n};\rho\nu_n r_0^n\right)}{\Gamma\left(2-\frac{1}{n}\right)}\cdot\|\Omega\|\rho^{1/n}. \quad (19)$$

To get the corresponding results for the simplices in the weighted Delaunay mosaic, we note that the number of vertices is $d_0^{1,n}=c_{0,0}^{1,n}+c_{0,1}^{1,n}$ and the number of edges is $d_1^{1,n}=c_{0,1}^{1,n}+c_{1,1}^{1,n}$. The two are the same, but this is not true if we limit the radius to a finite threshold. Indeed, the radius of a typical edge is Gamma distributed while the radius of a typical vertex follows a linear combination of two Gamma distributions. In the limit, when $n\to\infty$, the constants are

	$n=2$	3	4	5	6	7	8	9	...	20	...	∞
$C_{0,0}^{1,n}$	1.00	1.09	1.16	1.22	1.26	1.29	1.32	1.35	...	1.47	...	1.65
$C_{0,1}^{1,n}$	0.27	0.36	0.42	0.45	0.48	0.50	0.51	0.53	...	0.60	...	0.68
$D_{0}^{1,n}$	1.27	1.46	1.58	1.67	1.74	1.79	1.84	1.87	...	2.07	...	2.33

Table 1 The rounded constants in the expressions of the expected number of intervals and simplices of a 1-dimensional weighted Delaunay mosaic. The ratio of the expected number of critical edges over the expected number of regular edges it is monotonically decreasing. It follows that we can infer the ambient dimension from the ratio.

$\lim_{n\to\infty} C_{0,0}^{1,n} = \sqrt{e}$, $\lim_{n\to\infty} C_{0,1}^{1,n} = \sqrt{e}(\sqrt{2}-1)$, and $\lim_{n\to\infty} D_{0}^{1,n} = \lim_{n\to\infty} D_{1}^{1,n} = \sqrt{2e}$, which can again be verified using the Mathematica software.

Connection to Boolean model. Let X be a Poisson point process with density ρ in $\mathbb{R}^n$ and consider the union of closed balls of fixed radius r and centers in X, denoted X_r. The obtained random set is sometimes referred to as the *Boolean model* [22]. Write $X_r \cap \Omega$ for the intersection of this set with a line segment $\Omega \subseteq \mathbb{R}^1 \subseteq \mathbb{R}^n$. We claim that the homotopy type of this intersection is the same as that of the weighted Delaunay complex, restricted to Ω. In particular, $\beta_0(X_r \cap \Omega) = \beta_0(\mathrm{Del}_r(Y;\Omega))$, in which β_0 counts the connected components and $\mathrm{Del}_r(Y;\Omega)$ is the subcomplex of the weighted Delaunay mosaic that consists of all simplices with radius at most r lying completely within Ω. This follows from the general observation that the weighted Delaunay mosaic of a set of points $y \in \mathbb{R}^k$ with weights $w(y)$ is homotopy equivalent to the union of power balls, $Y_r = \{a \in \mathbb{R}^k \mid \|a-y\|^2 - w(y) \le r^2\}$, and $Y_r \cap \Omega = X_r \cap \Omega$. Indeed, the weighted Delaunay complex can be defined as the nerve of the decomposition of Y_r with the weighted Voronoi tessellation, so the Nerve Theorem asserts the homotopy equivalence; see [6] for details.

Following the evolution of the nested complexes $\mathrm{Del}_r(Y;\Omega)$, as r goes from 0 to ∞, we observe that every critical vertex creates a new component when it enters the complex, regular interval do not affect the homotopy type, and every critical edge connects two components; compare with Figure 3. It follows that the expected number of components in $X_r \cap \Omega$ is

$$\mathbb{E}[\beta_0(X_r \cap \Omega)] = \mathbb{E}[c_{0,0}^{1,n}(r) - c_{1,1}^{1,n}(r)] \tag{20}$$

$$= \tfrac{\sigma_{n-1}\Gamma(1-\frac{1}{n})}{n\nu_n^{1-1/n}} \left[\tfrac{\gamma(1-\frac{1}{n};\,\rho\nu_n r^n)}{\Gamma(1-\frac{1}{n})} - \tfrac{\gamma(2-\frac{1}{n};\,\rho\nu_n r^n)}{\Gamma(2-\frac{1}{n})} \right] \cdot \rho^{\frac{1}{n}} \|\Omega\| \tag{21}$$

$$= \tfrac{\sigma_{n-1}}{n\nu_n^{1-1/n}} \left[\gamma(1-\tfrac{1}{n};\,\rho\nu_n r^n) - \tfrac{\gamma(2-\frac{1}{n};\,\rho\nu_n r^n)}{1-\frac{1}{n}} \right] \cdot \rho^{\frac{1}{n}} \|\Omega\|. \tag{22}$$

We write $A = \rho\nu_n r^n$, use the definition of the incomplete Gamma function, and integrate by parts to get

$$\gamma(2-\tfrac{1}{n};\,A) = \int_0^A x^{1-\frac{1}{n}} e^{-x}\,\mathrm{d}x = \left[-x^{1-\frac{1}{n}}e^{-x}\right]_0^A + (1-\tfrac{1}{n}) \int_0^A x^{-\frac{1}{n}} e^{-x}\,\mathrm{d}x \tag{23}$$

$$= -A^{1-\frac{1}{n}}e^{-A} + (1-\tfrac{1}{n})\,\gamma(1-\tfrac{1}{n};\,A). \tag{24}$$

Noticing that $A^{1-\frac{1}{n}}\rho^{1/n} = (\rho\nu_n r^n)^{1-\frac{1}{n}}\rho^{1/n} = \rho\nu_n^{1-\frac{1}{n}} r^{n-1}$, we plug (24) into (22) to obtain

$$\mathbb{E}[\beta_0(X_r \cap \Omega)] = \tfrac{\sigma_{n-1}}{n\nu_n^{1-1/n}} \tfrac{1}{1-\frac{1}{n}} e^{-\rho\nu_n r^n} \rho\nu_n^{1-\frac{1}{n}} r^{n-1} \|\Omega\| = \tfrac{\sigma_{n-1}}{n-1} r^{n-1} e^{-\rho\nu_n r^n} \rho \|\Omega\| \tag{25}$$

$$= \nu_{n-1} r^{n-1} e^{-\rho\nu_n r^n} \rho \|\Omega\|, \tag{26}$$

where we use the identity $\frac{\sigma_{n-1}}{n-1} = \nu_{n-1}$ in the last transition. In short, (26) gives an explicit formula for the expected number of connected components in the Boolean model in $\mathbb{R}^n$ intersected with a line segment of length $\|\Omega\|$. While the authors did not find the explicit expression in the literature, this result is not new and follows after some straightforward computations from [10, Excercise 4.8]. The goal of this derivation is to provide another, more topological view on the problem. The graphs of β_0 for different dimensions n are shown in Figure 4. Using Crofton's formula [22, Theorem 9.4.7] but see also [11] and the fact

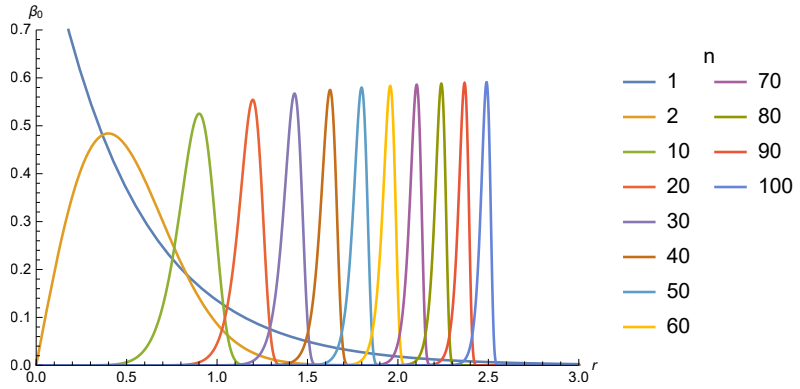

Figure 4 Graphs of the expected number of connected components per unit length depending on r, $\mathbb{E}[\beta_0(r)]$, for different dimensions n; that is: $\beta_0(r) = \beta_0(X_r \cap \Omega)$ with $\|\Omega\| = 1$ and $\rho = 1$. For increasing n, the graphs tend to get more focused, suggesting that the critical vertices get progressively more evenly spaced along the line.

that almost every connected component is a line segment, which meets the boundary of the Boolean model in two points, (26) can be transformed into a statement about its expected $(n-1)$-dimensional volume:

$$\overline{V}_{n-1}(X_r) = 2\sqrt{\pi}\,\frac{\Gamma\left(\frac{n}{2}\right)}{\Gamma\left(\frac{n+1}{2}\right)}\,\nu_{n-1} r^{n-1} e^{-\rho\nu_n r^n}\,\rho, \tag{27}$$

in which $\overline{V}_{n-1}(X_r)$ is the expected $(n-1)$-dimensional volume of the boundary of X_r inside a unit volume region; see [22, Section 9] for the detailed discussion of the quantity.

3 Anchored Blaschke–Petkantschin Formula

To extend the results in the previous section from 1 to k dimensions, we first generalize the Blaschke–Petkantschin formula for spheres stated as Theorem 7.3.1 in [22].

Setting the stage. Recall that $k \leq n$ are positive integers, and that we write $\mathbb{R}^k$ for the k-dimensional linear subspace spanned by the first k coordinate vectors of $\mathbb{R}^n$. While we used uppercase letters to denote simplices in the previous sections, we now write $\mathbf{x}$ for a sequence of $m+1 \leq k+1$ points in $\mathbb{R}^n$. The reason for the change of notation is that we integrate over all such sequences and do not limit ourselves to points in the Poisson point process. Similarly, we write $\mathbf{u}$ if the $m+1$ points lie on the unit sphere. As usual, we do not distinguish between a simplex and its vertices, so we write $\mathrm{Vol}_m(\mathbf{x})$ for the m-dimensional Lebesgue measure of the convex hull of $\mathbf{x}$. Assuming the $m+1$ points are in general position in $\mathbb{R}^n$, the affine hull of $\mathbf{x}$ is an m-plane, $M = \operatorname{aff}\mathbf{x}$. Furthermore, the set of centers of the spheres that pass through all points of $\mathbf{x}$ is an $(n-m)$-plane, $M^\perp$, orthogonal to M.

Generically, the intersection of $M^\perp$ with $\mathbb{R}^k$ is a plane of dimension $k-m$. The center of the smallest anchored sphere passing through $\mathbf{x}$ is the point of this intersection that is the closest to $\mathbf{x}$.

Top-dimensional case. We first show how to transform an integral over $m+1=k+1$ points to the integral over the unique anchored sphere passing through these points.

▶ **Lemma 2** (Blaschke–Petkantschin for Top-dimensional Simplices). *Let $0 \leq k \leq n$. Then every measurable non-negative function $f\colon (\mathbb{R}^n)^{k+1} \to \mathbb{R}$ satisfies*

$$\int\limits_{\mathbf{x}\in(\mathbb{R}^n)^{k+1}} f(\mathbf{x})\,\mathrm{d}\mathbf{x} = \int\limits_{y\in\mathbb{R}^k}\int\limits_{r\geq 0}\int\limits_{\mathbf{u}\in(\mathbb{S}^{n-1})^{k+1}} f(y+r\mathbf{u})r^{(n-1)(k+1)}k!\mathrm{Vol}_k(\mathbf{u}')\,\mathrm{d}\mathbf{u}\,\mathrm{d}r\,\mathrm{d}y, \tag{28}$$

in which $\mathbf{u}'$ is the projection of $\mathbf{u}$ to $\mathbb{R}^k$, $\mathrm{Vol}_k(\mathbf{u}')$ is the Lebesgue measure of the k-simplex, and we use the standard spherical measure on $\mathbb{S}^{n-1}$.

Proof. We follow the proof of Theorem 7.3.1 in [22], with just slight modifications. Recall first that we choose the coordinates in $\mathbb{R}^n$ so that the projection of $x=(x_1,x_2,\dots,x_n)$ to $\mathbb{R}^k \hookrightarrow \mathbb{R}^n$ is $x'=(x_1,\dots,x_k,0,\dots,0)$. The claimed relation is a change of variables: on the right-hand side, we represent the points $\mathbf{x}$ by the center $y\in\mathbb{R}^k \hookrightarrow \mathbb{R}^n$ of the anchored sphere passing through these points, its radius r, and k points $\mathbf{u}$ on the unit sphere $\mathbb{S}^{n-1}\hookrightarrow\mathbb{R}^n$. This change of variables is the mapping $\varphi\colon \mathbb{R}^k\times[0,\infty)\times(\mathbb{S}^{n-1})^{k+1}\to(\mathbb{R}^n)^{k+1}$ defined by $\varphi(y,r,\mathbf{u}_0,\mathbf{u}_1,\dots,\mathbf{u}_k)=(y+r\mathbf{u}_0,y+r\mathbf{u}_1,\dots,y+r\mathbf{u}_k)$, we note that φ is bijective up to a measure 0 subset of the domain. We claim the Jacobian of φ is

$$J(y,r,\mathbf{u}) = r^{(n-1)(k+1)}k!\mathrm{Vol}_k(\mathbf{u}'), \tag{29}$$

in which $\mathbf{u}'=(\mathbf{u}'_0,\mathbf{u}'_1,\dots,\mathbf{u}'_k)$ is the projection of $\mathbf{u}$ to $\mathbb{R}^k$. To prove (29) at a particular point $(y,r,\mathbf{u})$, we choose local coordinates around every point $\mathbf{u}_i$ on the sphere. We choose them such that the matrix $[\mathbf{u}_i\dot{\mathbf{u}}_i]$ is orthogonal, for every $0\leq i\leq k$, in which $\dot{\mathbf{u}}_i$ is the $n\times(n-1)$ matrix of partial derivatives with respect to the $n-1$ local coordinates. This is the same parametrization as in [22]. With this, the Jacobian is the absolute value of the $n(k+1)\times n(k+1)$ determinant:

$$J(y,r,\mathbf{u}) = \mathrm{abs}\left|\begin{array}{cc:ccc:c} E_{n,k} & \mathbf{u}_0 & r\dot{\mathbf{u}}_0 & 0 & \dots & 0 \\ E_{n,k} & \mathbf{u}_1 & 0 & r\dot{\mathbf{u}}_1 & \dots & 0 \\ \vdots & \vdots & \vdots & \vdots & \ddots & \vdots \\ E_{n,k} & \mathbf{u}_k & 0 & 0 & \dots & r\dot{\mathbf{u}}_k \end{array}\right|, \tag{30}$$

where we write the matrix in block notation, with $E_{n,k}$ the $n\times k$ matrix with all elements zero and ones in the diagonal. Similarly, $\mathbf{u}_i$ is a column vector of length n, $r\dot{\mathbf{u}}_i$ is an $n\times(n-1)$ matrix, and 0 is the zero matrix of appropriate size, which in this case is an $n\times(n-1)$ matrix. Like in [22], we extract r from $(k+1)(n-1)$ columns, and use the fact that transposing the matrix does not affect the determinant to get

$$\left(\frac{J(y,r,\mathbf{u})}{r^{(k+1)(n-1)}}\right)^2 = \left|\begin{array}{ccc:c} E_{k,n} & E_{k,n} & \dots & E_{k,n} \\ \mathbf{u}_0^T & \mathbf{u}_1^T & \dots & \mathbf{u}_k^T \\ \hdashline \dot{\mathbf{u}}_0^T & 0 & \dots & 0 \\ 0 & \dot{\mathbf{u}}_1^T & \dots & 0 \\ \vdots & \vdots & \ddots & \vdots \\ 0 & 0 & \dots & \dot{\mathbf{u}}_k^T \end{array}\right| \cdot \left|\begin{array}{cc:ccc:c} E_{n,k} & \mathbf{u}_0 & \dot{\mathbf{u}}_0 & 0 & \dots & 0 \\ E_{n,k} & \mathbf{u}_1 & 0 & \dot{\mathbf{u}}_1 & \dots & 0 \\ \vdots & \vdots & \vdots & \vdots & \ddots & \vdots \\ E_{n,k} & \mathbf{u}_k & 0 & 0 & \dots & \dot{\mathbf{u}}_0 \end{array}\right|. \tag{31}$$

The orthogonality of the matrices $[\mathbf{u}_i \dot{\mathbf{u}}_i]$ implies that $\mathbf{u}_i^T \mathbf{u}_i = 1$, $\dot{\mathbf{u}}_i^T \dot{\mathbf{u}}_i = E_{n-1,n-1}$, whereas $\mathbf{u}_i^T \dot{\mathbf{u}}_i$ is the zero row vector of length $n-1$, and $\dot{\mathbf{u}}_i^T \mathbf{u}_i$ is the zero column vector of length $n-1$, for each $0 \leq i \leq k$. We can therefore multiply the matrices and get

$$\left(\frac{J(y,r,\mathbf{u})}{r^{(k+1)(n-1)}}\right)^2 = \left|\begin{array}{cc:ccc} (k+1)E_{k,k} & \sum \mathbf{u}_i' & \dot{\mathbf{u}}_0' & \dots & \dot{\mathbf{u}}_k' \\ \sum \mathbf{u}_i'^T & k+1 & 0 & \dots & 0 \\ \hdashline \dot{\mathbf{u}}_0'^T & 0 & E_{n-1,n-1} & \dots & 0 \\ \vdots & \vdots & \vdots & \ddots & \vdots \\ \dot{\mathbf{u}}_k'^T & 0 & 0 & \dots & E_{n-1,n-1} \end{array}\right|, \tag{32}$$

in which we write $\mathbf{u}_i'$ for the vector consisting of the first k coordinates of $\mathbf{u}_i$. Similarly, $\dot{\mathbf{u}}_i'$ is the $k \times (n-1)$ matrix obtained from $\dot{\mathbf{u}}_i$ by dropping the bottom $n-k$ rows. As written, the $n(k+1) \times n(k+1)$ matrix in (32) is a $(k+3) \times (k+3)$ matrix of blocks, not all of the same size. To zero out the last $k+1$ blocks in the first row, we subtract the third row times $\dot{\mathbf{u}}_0'$, the fourth row times $\dot{\mathbf{u}}_1'$, and so on. The determinant is therefore the product of the determinants of the upper left 2×2 block matrix and the lower right $(k+1) \times (k+1)$ block matrix, the latter being 1. To further simplify the 2×2 block matrix, we use $[\mathbf{u}_i \dot{\mathbf{u}}_i][\mathbf{u}_i \dot{\mathbf{u}}_i]^T = E_{n,n}$, which implies $[\mathbf{u}_i' \dot{\mathbf{u}}_i'][\mathbf{u}_i' \dot{\mathbf{u}}_i']^T = E_{k,k}$, and we write the matrix as a product of two matrices:

$$\left(\frac{J(y,r,\mathbf{u})}{r^{(k+1)(n-1)}}\right)^2 = \left|\begin{array}{cc} (k+1)E_{k,k} - \sum \dot{\mathbf{u}}_i' \dot{\mathbf{u}}_i'^T & \sum \mathbf{u}_i' \\ \sum \mathbf{u}_i'^T & k+1 \end{array}\right| \tag{33}$$

$$= \left|\begin{array}{cc} \sum \mathbf{u}_i' \mathbf{u}_i'^T & \sum \mathbf{u}_i' \\ \sum \mathbf{u}_i'^T & k+1 \end{array}\right| = \left|\begin{bmatrix} \mathbf{u}_0' & \mathbf{u}_1' & \dots & \mathbf{u}_k' \\ 1 & 1 & \dots & 1 \end{bmatrix} \begin{bmatrix} \mathbf{u}_0'^T & 1 \\ \vdots & \vdots \\ \mathbf{u}_1'^T & 1 \\ \mathbf{u}_k'^T & 1 \end{bmatrix}\right|, \tag{34}$$

in which we get from (33) to (34) using $\dot{\mathbf{u}}_i' \dot{\mathbf{u}}_i'^T = E_{k,k} - \mathbf{u}_i' \mathbf{u}_i'^T$. Finally, the determinant of the vectors $\mathbf{u}_i'$ with appended 1 is $k!$ times the k-dimensional volume of $\mathbf{u}'$. Hence, $J(y,r,\mathbf{u}) = r^{(k+1)(n-1)} k! \mathrm{Vol}_k(\mathbf{u}')$, as claimed in (29). This completes the proof of (28). ◀

For $k = n$, this theorem is of course Theorem 7.3.1 in [22].

General case. Next we generalize to the case $m \leq k$. Recall that for a sequence $\mathbf{x}$ of $m+1 \leq k+1$ points in $\mathbb{R}^n$, there is a unique smallest anchored sphere passing through them. We claim that its center lies inside the orthogonal projection P of the m-dimensional affine hull of $\mathbf{x}$ onto $\mathbb{R}^k$. Indeed, orthogonally projecting the center of any anchored sphere passing through $\mathbf{x}$ to P in $\mathbb{R}^k$ we clearly get a point, which is a center of a smaller anchored sphere still passing through $\mathbf{x}$. The following theorem tells us how to integrate over these smallest anchored circumscribed spheres.

▶ **Theorem 3** (Anchored Blaschke–Petkantschin Formula). *Let $0 \leq m \leq k \leq n$ and $\alpha = n(m+1) - (k+1)$. Then every measurable non-negative function $f\colon (\mathbb{R}^n)^{m+1} \to \mathbb{R}$ satisfies*

$$\int_{\mathbf{x} \in (\mathbb{R}^n)^{m+1}} f(\mathbf{x}) \, \mathrm{d}\mathbf{x} = \int_{y \in \mathbb{R}^k} \int_{P \in \mathcal{L}_m^k} \int_{r \geq 0} \int_{\mathbf{u} \in (S)^{m+1}} f(y + r\mathbf{u}) r^\alpha [m! \mathrm{Vol}_m(\mathbf{u}')]^{k-m+1} \, \mathrm{d}\mathbf{u} \, \mathrm{d}r \, \mathrm{d}P \, \mathrm{d}y, \tag{35}$$

in which $\mathcal{L}_m^k$ is the Grassmannian of (linear) m-planes in $\mathbb{R}^k$, $\mathbf{u}'$ is the projection of $\mathbf{u}$ to P, and S is short for the unit sphere in $P \times \mathbb{R}^{n-k}$.

Proof. We use Blaschke–Petkantschin formula twice, first in its standard form. For $P \in \mathcal{L}^k_m$, we write $P \times \mathbb{R}^{n-k} \in \mathcal{L}^n_{m+n-k}$ for the $(m+n-k)$-plane whose orthogonal projection to $\mathbb{R}^k$ is P. The first application of Blaschke–Petkantschin formula integrates over all (affine) m-planes in $\mathbb{R}^k$, spanned by the projections of $\mathbf{x}$ to $\mathbb{R}^k$:

$$\int\limits_{\mathbf{x}\in(\mathbb{R}^n)^{m+1}} f(\mathbf{x})\,\mathrm{d}\mathbf{x} = \int\limits_{P\in\mathcal{L}^k_m}\int\limits_{h\in P^\perp}\int\limits_{\mathbf{x}\in(P\times\mathbb{R}^{n-k})^{m+1}} f(h+\mathbf{x})[m!\mathrm{Vol}_m(\mathbf{x}')]^{k-m}\,\mathrm{d}\mathbf{x}\,\mathrm{d}h\,\mathrm{d}P. \tag{36}$$

For every m-plane P in $\mathbb{R}^k$, we consider the vertical $(m+n-k)$-plane $P\times\mathbb{R}^{n-k}$ in $\mathbb{R}^n$ and apply Lemma 2 inside it. Recalling that S is the unit sphere in $P\times\mathbb{R}^{n-k}$, this gives

$$\int\limits_{\mathbf{x}\in(\mathbb{R}^n)^{m+1}} f(\mathbf{x})\,\mathrm{d}\mathbf{x} = \int\limits_{P\in\mathcal{L}^k_m}\int\limits_{h\in P^\perp}\int\limits_{z\in P}\int\limits_{r\geq 0}\int\limits_{\mathbf{u}\in(S)^{m+1}} f(h+z+r\mathbf{u})r^{(m+n-k-1)(m+1)} \tag{37}$$

$$m!\mathrm{Vol}_m(\mathbf{u}')[m!\mathrm{Vol}_m(r\mathbf{u}')]^{k-m}\,\mathrm{d}\mathbf{u}\,\mathrm{d}r\,\mathrm{d}z\,\mathrm{d}h\,\mathrm{d}P. \tag{38}$$

Note that $\mathrm{Vol}_m(r\mathbf{u}') = r^m\mathrm{Vol}_m(\mathbf{u}')$, which implies that the final power of r is $(m+n-k-1)(m+1)+m(k-m) = \alpha$. Finally, we get the claimed relation by setting $y = z+h$ and exchanging the integral over $P\in\mathcal{L}^k_m$ with the integral over $y\in\mathbb{R}^k$. ◀

4 Expected Number of Intervals

In this section, we use the anchored Blaschke–Petkantschin formula of the previous section to compute the expected numbers of intervals of a weighted Delaunay mosaic in $\mathbb{R}^k$. We do this for every type and use a radius threshold to get more detailed probabilistic information. Recall that the weighted mosaic is a random k-dimensional slice of the (unweighted) Poisson–Delaunay mosaic with density $\rho > 0$ in $\mathbb{R}^n$.

Slivnyak–Mecke formula. To count the type (ℓ, m) intervals, we focus our attention by restricting the center of the circumsphere to a region $\Omega\subseteq\mathbb{R}^k$ and the radius to be less than or equal r_0. Any sequence $\mathbf{x} = (\mathbf{x}_0, \mathbf{x}_1, \ldots, \mathbf{x}_m)$ of $m+1$ points in $\mathbb{R}^n$ defines such an interval if it satisfies the following conditions:

1. the smallest anchored sphere passing through $\mathbf{x}$ is empty, writing $\mathbb{P}_\emptyset(\mathbf{x})$ for the probability of this event;
2. the center z of this sphere lies in Ω, writing $\mathbf{1}_\Omega(\mathbf{x})$ for the indicator;
3. the radius r of this sphere is bounded from above by r_0, writing $\mathbf{1}_{r_0}(\mathbf{x})$ for the indicator;
3. the origin of $\mathbb{R}^k$ sees exactly $m-\ell$ facets of the projected m-simplex from the outside, writing $\mathbf{1}_{m-\ell}(\mathbf{x})$ for the indicator.

These are the same conditions as in [7] and [3] with the only difference that the sphere is now required to be anchored, and modulo this remark the proofs are identical. Combining these conditions with the Slivnyak–Mecke formula, we get an integral expression for the expected

number of type (ℓ, m) intervals, which we partially evaluate using Theorem 3 and Lemma 4:

$$\mathbb{E}[c^{k,n}_{\ell,m}(r_0)] = \tfrac{1}{(m+1)!} \int_{\mathbf{x}\in(\mathbb{R}^n)^{m+1}} \mathbb{P}_\emptyset(\mathbf{x})\mathbf{1}_\Omega(\mathbf{x})\mathbf{1}_{r_0}(\mathbf{x})\mathbf{1}_{m-\ell}(\mathbf{x})\,\mathrm{d}\mathbf{x} \tag{39}$$

$$= \|\Omega\|\|\mathcal{L}^k_m\|\rho^{m+1}\tfrac{m!^{k-m+1}}{(m+1)!} \int_{r\le r_0} e^{-\rho\nu_n r^n} r^\alpha\,\mathrm{d}r \int_{\mathbf{u}\in(S)^{m+1}} \mathbf{1}_{m-\ell}(\mathbf{u})\mathrm{Vol}_m(\mathbf{u}')^{k-m+1}\,\mathrm{d}\mathbf{u} \tag{40}$$

$$= \|\Omega\|\rho^{\frac{k}{n}}\tfrac{m!^{k-m}}{m+1}\|\mathcal{L}^k_m\|\tfrac{\gamma\left(m+1-\frac{k}{n};\,\rho\nu_n r_0^n\right)}{n\nu_n^{m+1-\frac{k}{n}}} \int_{\mathbf{u}\in(S)^{m+1}} \mathbf{1}_{m-\ell}(\mathbf{u})\mathrm{Vol}_m(\mathbf{u}')^{k-m+1}\,\mathrm{d}\mathbf{u} \tag{41}$$

$$= C^{k,n}_{\ell,m}\cdot\tfrac{\gamma\left(m+1-\frac{k}{n};\,\rho\nu_n r_0^n\right)}{\Gamma\left(m+1-\frac{k}{n}\right)}\cdot\|\Omega\|\rho^{\frac{k}{n}}. \tag{42}$$

Specifically, we get (40) by noting $\mathbb{P}_\emptyset(\mathbf{x}) = e^{-\rho\nu_n r^n}$, applying Theorem 3 to the right-hand side of (39), collapsing the indicators, using rotational invariance, and writing S for the unit sphere in $\mathbb{R}^{m+n-k}$. We get (41) from (40) by applying Lemma 4 with $j = \alpha+1 = n(m+1)-k$, $c = \rho\nu_n$, $p = n$, $t_0 = r_0$, which asserts that the integral over the radius evaluates to the fraction involving the incomplete Gamma function. Finally, we get (42) by defining the constant

$$C^{k,n}_{\ell,m} = \tfrac{m!^{k-m}\|\mathcal{L}^k_m\|\Gamma\left(m+1-\frac{k}{n}\right)}{(m+1)n\nu_n^{m+1-\frac{k}{n}}} \int_{\mathbf{u}\in(S)^{m+1}} \mathbf{1}_{m-\ell}(\mathbf{u})\mathrm{Vol}_m(\mathbf{u}')^{k-m+1}\,\mathrm{d}\mathbf{u}. \tag{43}$$

As a sanity check, we set $\ell = m = 0$ and $k = 1$, and get $C^{1,n}_{0,0} = \sigma_{n-1}\Gamma(1-1/n)/(n\nu_n^{1-1/n})$ because $S \subseteq \mathbb{R}^{n-1}$ has volume σ_{n-1}, and we have $\mathbf{1}_0(\mathbf{u}_0) = 1$ and $\mathrm{Vol}_0(\mathbf{u}_0) = 1$ for all points $\mathbf{u}_0 \in S$. This agrees with (15) in Section 2.

Simplices in the weighted Delaunay mosaic. Since this constant in (43) does not depend on r_0, we deduce that the radius of a typical type (ℓ, m) interval is Gamma distributed. The radius of a typical j-simplex in the weighted Poisson–Delaunay mosaic therefore follows a linear combination of Gamma distributions. Indeed, we get the total number of j-simplices as $d^{k,n}_j = \sum_{\ell=0}^{j}\sum_{m=j}^{k}\binom{m-\ell}{m-j}c^{k,n}_{\ell,m}$; see [7]. The same relation holds if we limit the simplices to radius at most r_0, and also if we replace the simplex counts by the constants $C^{k,n}_{\ell,m}$ and the analogously defined $D^{k,n}_j$. Before continuing, we consider the top-dimensional case, $j = k$, in which $D^{k,n}_k = \sum_{\ell=0}^{k} C^{k,n}_{\ell,k}$. Taking the sum eliminates the indicator function in (43), and we get

$$D^{k,n}_k = \frac{\Gamma\left(k+1-\frac{k}{n}\right)}{(k+1)n\nu_n^{k+1-\frac{k}{n}}} \int_{\mathbf{u}\in(\mathbb{S}^{n-1})^{k+1}} \mathrm{Vol}_k(\mathbf{u}')\,\mathrm{d}\mathbf{u}. \tag{44}$$

We can compare this with the expression for the number of Voronoi vertices by Møller [18] using Crofton's formula [11, Chapter 6]; see also [22, Theorem 10.2.4]. By duality, the number of vertices in the weighted Voronoi tessellation is the number of top-dimensional simplices in the weighted Delaunay mosaic. Each vertex is the intersection of an $(n-k)$-dimensional Voronoi polyhedron with the k-plane, and if we know the expected number of intersections, then we also know the integral, over all k-planes. Crofton's formula applies and gives the $(n-k)$-dimensional volume of the $(n-k)$-skeleton of the Voronoi tessellation as $\sigma_n/(2\|\mathcal{L}^n_k\|\nu_{n-1})$ times the mentioned integral. It turns out that the expected volume is not so difficult to compute otherwise, so we can turn the argument around and deduce the

expected number of vertices from the expected $(n-k)$-dimensional volume. This gives

$$D_k^{k,n} = \frac{\sigma_1\sigma_{n+1}}{\sigma_{k+1}\sigma_{n-k+1}} \frac{2^{k+1}\pi^{k/2}}{n(k+1)!} \frac{\Gamma\big(\frac{kn+n-k+1}{2}\big)}{\Gamma\big(\frac{kn+n-k}{2}\big)} \frac{\Gamma\big(\frac{n+2}{2}\big)^{k+1-\frac{k}{n}}}{\Gamma\big(\frac{n+1}{2}\big)^k} \frac{\Gamma\big(k+1-\frac{k}{n}\big)}{\Gamma\big(\frac{n-k+1}{2}\big)}. \tag{45}$$

Comparing (45) with (44), we get an explicit expression for the expected k-dimensional volume of the projection of a random k-simplex inscribed in $\mathbb{S}^{n-1}$.

5 Computations

We now return to (43) and note that the integral on the right-hand side is σ_{m+n-k}^{m+1} times the expected value of the random variable

$$U_{\ell,m}^{k,n} = \mathbf{1}_{m-\ell}(\mathbf{u})\mathrm{Vol}_m(\mathbf{u}')^{k-m+1}, \tag{46}$$

where $\mathbf{u}$ is a sequence of $m+1$ random points uniformly and independently distributed on the unit sphere in $\mathbb{R}^{m+n-k}$, and $\mathbf{u}'$ is the corresponding sequence of points projected to $\mathbb{R}^m \hookrightarrow \mathbb{R}^{m+n-k}$. Our goal is to compute $\mathbb{E}[U_{\ell,m}^{k,n}]$ in some special cases. Instead of working with the original points, we prefer to study their projections to $\mathbb{R}^m$, but the distribution of the $m+1$ points in $\mathbb{R}^m$ has yet to be determined. If the upper bound is a vertex or an edge, then we find explicit expressions of the expected number of intervals.

Critical vertices. For $m=0$, we count intervals of type $(0,0)$ or, equivalently, critical vertices. Since $U_{0,0}^{k,n}=1$, for all $k \le n$, we get

$$C_{0,0}^{k,n} = \sigma_{n-k}\frac{\Gamma\big(1-\frac{k}{n}\big)}{n\nu_n^{1-k/n}} \tag{47}$$

from (43). Accordingly, the expected number of critical vertices in Ω with radius at most r_0 is $C_{0,0}^{k,n}$ times the normalized incomplete Gamma function times $\|\Omega\|\rho^{k/n}$; compare with (5) and (6) in Section 2.

Vertex-edge pairs. Next we count the intervals of type $(0,1)$ or, equivalently, the regular vertex-edge pairs. For this, we need the expectation of $U_{0,1}^{k,n}$: picking two random points on the unit sphere in $\mathbb{R}^{n-k+1}$ and projecting them to $\mathbb{R}^1 \hookrightarrow \mathbb{R}^{n-k+1}$, this is the expectation when we get the k-th power of the distance between the projected points, if they lie on the same side of the origin, and we get 0, otherwise. Writing $\mathbf{u}_0', \mathbf{u}_1' \in [-1,1]$ for the projected points and $x=|\mathbf{u}_0'|$, $y=|\mathbf{u}_1'|$ for their absolute values, we note that the signs and magnitudes are independent. It follows that we get zero with probability $\frac{1}{2}$, so the desired expectation is

$$\mathbb{E}[U_{0,1}^{k,n}] = \tfrac{1}{2}\mathbb{E}[|x-y|^k] = \mathbb{E}[(x-y)^k\mathbf{1}_{x>y}]. \tag{48}$$

We can therefore restrict our attention to the half of the unit sphere that projects to $[0,1]$. To integrate over this hemisphere, we use that x^2 and y^2 are independent Beta-distributed random variables; see Appendix A. Setting $a=x^2$ and $b=y^2$, we have

$$\mathbb{E}[U_{0,1}^{k,n}] = \frac{1}{B\big(\frac{n-k}{2},\frac{1}{2}\big)^2}\int_{a=0}^{1}\int_{b=0}^{a}[\sqrt{a}-\sqrt{b}]^k a^{-\frac{1}{2}}(1-a)^{\frac{n-k-2}{2}}b^{-\frac{1}{2}}(1-b)^{\frac{n-k-2}{2}}\,\mathrm{d}a\,\mathrm{d}b \tag{49}$$

$$= \frac{4}{B\big(\frac{n-k}{2},\frac{1}{2}\big)^2}\int_{x=0}^{1}\int_{y=0}^{x}[x-y]^k(1-x^2)^{\frac{n-k-2}{2}}(1-y^2)^{\frac{n-k-2}{2}}\,\mathrm{d}x\,\mathrm{d}y \tag{50}$$

$$= \frac{\Gamma(k+1)\Gamma\big(\frac{n-k+1}{2}\big)^2}{2^k\sqrt{\pi}\Gamma\big(\frac{n-k}{2}\big)}\cdot {}_3\tilde{F}_2\left(\tfrac{1}{2},1,\tfrac{k-n+2}{2};\,\tfrac{k+3}{2},\tfrac{n+2}{2};\,1\right), \tag{51}$$

in which ${}_3\tilde{F}_2$ is the regularized hypergeometric function considered in Appendix A and we use the Mathematica software to get from (50) to (51). As mentioned at the end of this appendix, $\frac{k+3}{2} + \frac{n+2}{2} > \frac{1}{2} + 1 + \frac{k-n+2}{2}$ is a sufficient condition for the convergence of the infinite sum that defines the value of the regularized hypergeometric function. This is equivalent to $n > 0$, which is always satisfied. Plugging (51) into (43), we get an expression for the corresponding constant:

$$C_{0,1}^{k,n} = \frac{\sigma_{n-k+1}^2 \sigma_k \Gamma\big(2 - \frac{k}{n}\big)}{4n\nu_n^{2-k/n}} \frac{\Gamma(k+1)\Gamma\big(\frac{n-k+1}{2}\big)^2}{2^k\sqrt{\pi}\Gamma\big(\frac{n-k}{2}\big)} \cdot {}_3\tilde{F}_2\left(\tfrac{1}{2}, 1, \tfrac{k-n+2}{2}; \tfrac{k+3}{2}, \tfrac{n+2}{2}; 1\right). \tag{52}$$

Critical edges. Next we count the intervals of type $(1,1)$ or, equivalently, the critical edges. Here the expectation of $U_{1,1}^{k,n}$ is relevant: picking two points on the unit sphere in $\mathbb{R}^{n-k+1}$ and projecting them to $\mathbb{R}^1 \hookrightarrow \mathbb{R}^{n-k+1}$, this is the expectation in which we get the k-th power of the distance between the projected points, if they lie on opposite sides of the origin, and we get 0, otherwise. Using again that the signs and magnitude of the projected points are independent, we note that this expectation is $\mathbb{E}[U_{1,1}^{k,n}] = \frac{1}{2}\mathbb{E}[(x+y)^k]$. Setting $a = x^2$, $b = y^2$, and integrating as before, we get

$$\mathbb{E}[U_{1,1}^{k,n}] = \frac{1}{B\big(\frac{n-k}{2}, \frac{1}{2}\big)^2} \int_{a=0}^{1}\int_{b=0}^{1} \Big[\sqrt{a} + \sqrt{b}\Big]^k a^{-\frac{1}{2}}(1-a)^{\frac{n-k-2}{2}} b^{-\frac{1}{2}}(1-b)^{\frac{n-k-2}{2}} \,\mathrm{d}a\,\mathrm{d}b \tag{53}$$

$$= \frac{1}{B\big(\frac{n-k}{2}, \frac{1}{2}\big)^2} \int_{a=0}^{1}\int_{b=0}^{1} \sum_{i=0}^{k} \binom{k}{i} a^{\frac{i-1}{2}} b^{\frac{k-i-1}{2}} (1-a)^{\frac{n-k-2}{2}} (1-b)^{\frac{n-k-2}{2}} \,\mathrm{d}a\,\mathrm{d}b \tag{54}$$

$$= \frac{1}{B\big(\frac{n-k}{2}, \frac{1}{2}\big)^2} \sum_{i=0}^{k} \binom{k}{i} B\big(\tfrac{n-k}{2}, \tfrac{i+1}{2}\big) B\big(\tfrac{n-k}{2}, \tfrac{k-i+1}{2}\big). \tag{55}$$

Plugging (55) into (43), we get the expression for the corresponding constant:

$$C_{1,1}^{k,n} = \frac{\sigma_{n-k+1}^2 \sigma_k \Gamma\big(2 - \frac{k}{n}\big)}{8n\nu_n^{2-k/n} B\big(\frac{n-k}{2}, \frac{1}{2}\big)^2} \sum_{i=0}^{k} \binom{k}{i} B\big(\tfrac{n-k}{2}, \tfrac{i+1}{2}\big) B\big(\tfrac{n-k}{2}, \tfrac{k-i+1}{2}\big). \tag{56}$$

Constants in low dimensions. The authors have checked the k-dimensional formulas against the 1-dimensional formulas in Section 2, both symbolically and numerically. In $k = 2$ dimensions, the formulas provide sufficient information to compute all constants governing the expectations of the six types of intervals. We get three constants from (47), (52), (56):

$$C_{0,0}^{2,n} = \frac{\sigma_{n-2}\Gamma\big(1 - \frac{2}{n}\big)}{n\nu_n^{1-2/n}}, \tag{57}$$

$$C_{0,1}^{2,n} = \frac{\sigma_{n-1}^2\sqrt{\pi}\Gamma\big(2 - \frac{2}{n}\big)}{4n\nu_n^{2-2/n}} \frac{\Gamma\big(\frac{n-1}{2}\big)^2}{\Gamma\big(\frac{n-2}{2}\big)} \cdot {}_3\tilde{F}_2\left(\tfrac{1}{2}, 1, \tfrac{4-n}{2}; \tfrac{5}{2}, \tfrac{n+2}{2}; 1\right), \tag{58}$$

$$C_{1,1}^{2,n} = \frac{\sigma_{n-1}^2\Gamma\big(2 - \frac{2}{n}\big)\pi}{2n\nu_n^{2-2/n}} \cdot \left[\frac{1}{n-1} + \frac{\Gamma\big(\frac{n-1}{2}\big)^2}{\pi\Gamma\big(\frac{n}{2}\big)^2}\right]. \tag{59}$$

The critical simplices satisfy the Euler relation [8]: $C_{0,0}^{2,n} - C_{1,1}^{2,n} + C_{2,2}^{2,n} = 0$, which gives us the constant for the critical triangles. We get another linear relation from the fact that in the plane the number of triangles is twice the number of vertices [22, page 458, Theorem 10.1.2]:

$C^{2,n}_{0,2} + C^{2,n}_{1,2} + C^{2,n}_{2,2} = 2(C^{2,n}_{0,0} + C^{2,n}_{0,1} + C^{2,n}_{0,2})$. Finally, we get a relation for the number of weighted Delaunay triangles from (45), which we restate for $k = 2$:

$$D^{2,n}_2 = \frac{2\sigma_{n+1}}{3n\sigma_{n-1}} \frac{\Gamma\big(\frac{3n-1}{2}\big)}{\Gamma\big(\frac{3n-2}{2}\big)} \frac{\Gamma\big(\frac{n+2}{2}\big)^{3-\frac{2}{n}}}{\Gamma\big(\frac{n+1}{2}\big)^2} \frac{\Gamma\big(3-\frac{2}{n}\big)}{\Gamma\big(\frac{n-1}{2}\big)}. \tag{60}$$

Combining $C^{2,n}_{0,2} + C^{2,n}_{1,2} + C^{2,n}_{2,2} = D^{2,n}_2$ with the two linear relations mentioned above, we get

$$C^{2,n}_{0,2} = -C^{2,n}_{0,0} - C^{2,n}_{0,1} + \tfrac{1}{2} D^{2,n}_2, \tag{61}$$

$$C^{2,n}_{1,2} = C^{2,n}_{0,0} + C^{2,n}_{0,1} - C^{2,n}_{2,2} + \tfrac{1}{2} D^{2,n}_2, \tag{62}$$

$$C^{2,n}_{2,2} = -C^{2,n}_{0,0} + C^{2,n}_{1,1}. \tag{63}$$

For small values of n, the constants are approximated in Table 2.

	$n=3$	4	5	6	7	8	9	10	...	20	...	1000
$C^{2,n}_{0,0}$	1.11	1.25	1.38	1.49	1.58	1.66	1.73	1.79	...	2.12	...	2.69
$C^{2,n}_{0,1}$	0.26	0.42	0.54	0.63	0.71	0.77	0.82	0.86	...	1.12	...	1.54
$C^{2,n}_{0,2}$	0.09	0.15	0.21	0.25	0.28	0.31	0.33	0.35	...	0.47	...	0.65
$C^{2,n}_{1,1}$	2.47	2.92	3.30	3.61	3.87	4.09	4.28	4.44	...	5.37	...	6.92
$C^{2,n}_{1,2}$	1.46	1.83	2.13	2.37	2.57	2.74	2.89	3.01	...	3.72	...	4.88
$C^{2,n}_{2,2}$	1.37	1.67	1.92	2.12	2.29	2.43	2.55	2.66	...	3.25	...	4.23
$D^{2,n}_0$	1.46	1.83	2.13	2.37	2.57	2.74	2.89	3.01	...	3.72	...	4.88
$D^{2,n}_1$	4.37	5.48	6.38	7.10	7.71	8.22	8.66	9.03	...	11.16	...	14.65
$D^{2,n}_2$	2.92	3.66	4.25	4.74	5.14	5.48	5.77	6.02	...	7.44	...	9.77

Table 2 The rounded constants in the expressions of the expected number of intervals and simplices of a 2-dimensional weighted Delaunay mosaic obtained from a Poisson point process in n dimensions.

6 Discussion

The main result of this paper is the stochastic analysis of the radius function of a weighted Poisson–Delaunay mosaic. As a consequence, we get formulas for the expected number of simplices in weighted Poisson-Delaunay mosaics; compare with [13, 14]. The main technical steps leading up to this result are a new Blaschke–Petkantschin formula for spheres, stated as Theorem 3, and the discrete Morse theory approach recently introduced in [7]. There are a number of open questions that remain:

- We have explicit expressions for the constants in the expected number of intervals of all types for dimension $k \leq 2$. To go beyond two dimensions, Wendel's method of reflecting vertices of a simplex through the origin [25] should be useful. Short of getting precise formulas, can we say something about the asymptotic behavior of the constants, as k and n go to infinity?
- The connection to Crofton's formula and the volumes of Voronoi skeleta has been mentioned in Section 4. Are there further connections that relate such volumes with simplices of dimension strictly less than k, or with subsets of simplices limited to radii at most r_0?
- The slice construction implies a repulsive force among the vertices: the vertices of the weighted Poisson–Delaunay mosaic are more evenly spread than a Poisson point process. For fixed k, the repulsion gets stronger with increasing n. It would be interesting to study this repulsive force and its consequences analytically.

References

1 F. Aurenhammer. Power diagrams: properties, algorithms, and applications. *SIAM J. Comput.* **16** (1987) 93–105.

2 F. Aurenhammer and H. Imai. Geometric relations among Voronoi diagrams. *Geometriae Dedicata* **27** (1988), 65–75.

3 U. Bauer and H. Edelsbrunner. The Morse theory of Čech and Delaunay complexes. *Trans. Amer. Math. Soc.* **369** (2017), 3741-3762.

4 L. Burtseva, F. Werner, B. Valdez, A. Pestriakov, R. Romero and V. Petranovskii. Tessellation methods for modeling material structure. *Appl. Math. Mech.* **756** (2015), 426–435.

5 H. Edelsbrunner. *Geometry and Topology for Mesh Generation.* Cambridge Univ. Press, Cambridge, England, 2001.

6 Edelsbrunner, H. and Harer, J.L. (2010). *Computational Topology. An Introduction.* Amer. Math. Soc., Providence, Rhode Island.

7 H. Edelsbrunner, A. Nikitenko and M. Reitzner. Expected sizes of Poisson–Delaunay mosaics and their discrete Morse functions. *Adv. Appl. Prob.*, to appear.

8 R. Forman. Morse theory for cell complexes. *Adv. Math.* **134** (1998), 90–145.

9 I.M. Gelfand, M.M. Kapranov and A.V. Zelevinsky. *Discriminants, Resultants, and Multidimensional Determinants.* Birkhäuser, Boston, Massachusetts, 1994.

10 P. Hall. *Introduction to the Theory of Coverage Processes.* Wiley, New York, USA, 1988.

11 H. Hadwiger. *Vorlesungen üer Inhalt, Oberfläche und Isoperimetrie.* Die Grundlehren der Mathematischen Wissenschaften, vol. **93**. Springer, Berlin, Germany, 1957.

12 J.F.C. Kingman. *Poisson Processes.* Oxford Univ. Press, Oxford, England, 1993.

13 C. Lautensack. *Random Laguerre Tessellations.* Ph.D. thesis, Dept. Math., Univ. Karlsruhe, Germany, 2007.

14 C. Lautensack and S. Zuyev. Random Laguerre tessellations. *Adv. Appl. Prob. (SGSA)* **40** (2008), 630–650.

15 S. Li. Concise formulas for the area and volume of a hyperspherical cap. *Asian J. Math. Stat.* **4** (2011), 66–70.

16 R.E. Miles. On the homogeneous planar Poisson point process. *Math. Biosci.* **6** (1970), 85–127.

17 R.E. Miles. Isotropic random simplices. *Adv. Appl. Prob.* **3** (1971), 353–382.

18 Møller, J. Random tessellations in $\mathbb{R}^d$. *Adv. Appl. Prob.* **21** (1989), 37–73.

19 A. Okabe, B. Boots, K. Sugihara and S.N. Chui. *Spatial Tessellations: Concepts and Applications of Voronoi Diagrams.* Second edition, John Wiley & Sons, Chicester, England, 2000.

20 F.W. Olver, D.W. Lozier, R.F. Boisvert and C.W. Clark. *NIST Handbook of Mathematical Functions.* Cambridge University Press, New York, 2010.

21 N. Prunet and E.M. Meyerowitz. Genetics and plant development. *C. R. Biologies*, to appear.

22 R. Schneider and W. Weil. *Stochastic and Integral Geometry.* Springer, Berlin, Germany, 2008.

23 R. Sibson. A vector identity for the Dirichlet tessellation. *Math. Proc. Camb. Phil. Soc.* **87** (1980), 151–155.

24 C. Walck. *Handbook on Statistical Distributions for Experimentalists.* Internal Report SUFPFY/9601 Stockholm, 1996.

25 J.G. Wendel. A problem in geometric probability. *Math. Scand.* **11** (1962), 109–111.

A On Special Functions

In this appendix, we define and discuss three types of special functions used in the main body of this paper: Gamma functions, Beta functions, and hypergeometric functions.

Gamma functions. We recall that the *lower-incomplete Gamma function* takes two parameters, j and $t_0 \geq 0$, and is defined by

$$\gamma(j;\, t_0) = \int_{t=0}^{t_0} t^{j-1} e^{-t} \, \mathrm{d}t. \tag{64}$$

The corresponding complete *Gamma function* is $\Gamma(j) = \gamma(j;\, \infty)$. An important relation for Gamma functions is $\Gamma(j+1) = j\Gamma(j)$, which holds for any real j that is not a non-positive integer. We often use the ratio, $\gamma(j;\, t_0)/\Gamma(j)$, which is the density of a probability distribution and called the *Gamma distribution* with parameter j. We prove a technical lemma about incomplete Gamma functions, which is repeatedly used in the main body of this paper.

▶ **Lemma 4** (Gamma Function). *Let $c, p, j, t_0 \in \mathbb{R}$ with $p \neq 0$ and $t_0 > 0$. Then*

$$\int_{t=0}^{t_0} t^{j-1} e^{-ct^p} \, \mathrm{d}t = \frac{\gamma\left(\frac{j}{p};\, ct_0^p\right)}{pc^{j/p}}. \tag{65}$$

Proof. We rewrite the numerator of the right-hand side of (65) using the definition of the right-incomplete Gamma function (64) and substituting $u = ct^p$ and $\mathrm{d}u = cpt^{p-1} \, \mathrm{d}t$:

$$\gamma\left(\tfrac{j}{p};\, ct_0^p\right) = \int_{u=0}^{ct_0^p} u^{\frac{j}{p}-1} e^{-u} \, \mathrm{d}u \tag{66}$$

$$= \int_{t=0}^{t_0} (ct^p)^{\frac{j}{p}-1} e^{-ct^p} cpt^{p-1} \, \mathrm{d}t \tag{67}$$

$$= \int_{t=0}^{t_0} pc^{\frac{j}{p}} t^{j-1} e^{-ct^p} \, \mathrm{d}t. \tag{68}$$

Dividing by $pc^{j/p}$ gives the claimed relation. ◀

Beta functions. Given real numbers a, b, and $0 \leq t_0 \leq 1$, the *incomplete Beta function* is defined by

$$B_{t_0}(a, b) = \int_{t=0}^{t_0} t^{a-1}(1-t)^{b-1} \, \mathrm{d}t, \tag{69}$$

and the complete *Beta function* is $B(a, b) = B_1(a, b)$, which can be expressed in terms of complete Gamma functions: $B(a, b) = \Gamma(a)\Gamma(b)/\Gamma(a+b)$.

The Beta functions can be used to integrate over the projection of a sphere in $\mathbb{R}^n$ to a linear subspace $\mathbb{R}^k \hookrightarrow \mathbb{R}^n$, as we now explain. Assuming $\mathbb{R}^k$ is spanned by the first k coordinate vectors of $\mathbb{R}^n$, the projection of a point means dropping coordinates $k+1$ to n. Suppose now that we pick a point $x = (x_1, x_2, \ldots, x_n)$ uniformly on $\mathbb{S}^{n-1}$ by normalizing a vector of n normally distributed random variables: $X_i \sim \mathcal{N}(0, 1)$ for $1 \leq i \leq n$ and $x_j = X_j / \left(\sum_{i=1}^n X_i^2\right)^{1/2}$ for $1 \leq j \leq n$. Its projection to $\mathbb{R}^k$ is $x' = (x_1, \ldots, x_k, 0, \ldots, 0)$, and the squared distance from the origin is $\|x'\|^2 = \left(\sum_{i=1}^k x_i^2\right) / \left(\sum_{i=1}^n x_i^2\right)$. It can be written as $r^2 = X/(X+Y)$, in which X and Y are χ^2-distributed independent random variables with k and $n-k$ degrees of freedom, respectively. This implies that $r^2 \sim B\left(\frac{k}{n}, \frac{n-k}{n}\right)$ [24, Section

4.2]. Consider for example the case $k = n - 1$. Integrating in $\mathbb{R}^k$ over all points with distance at most r_0 from the origin is the same as integrating over two spherical caps of $\mathbb{S}^{n-1}$, namely the cap around the north-pole bounded by $(n-2)$-spheres of radius r_0, and a similar cap around the south-pole. To compute the volume of a single such cap, we set $t_0 = r_0^2$ and integrate the incomplete Beta function:

$$\mathrm{Vol}_{n-1}(r_0) = \frac{\sigma_n}{2B\left(\frac{n-1}{2}, \frac{1}{2}\right)} \int_{t=0}^{t_0} t^{\frac{n-1}{2}-1}(1-t)^{\frac{1}{2}-1}\,\mathrm{d}t = \frac{B_{t_0}\left(\frac{n-1}{2}, \frac{1}{2}\right)}{2B\left(\frac{n-1}{2}, \frac{1}{2}\right)}. \tag{70}$$

Similarly, we can integrate over a ball in a k-dimensional projection and get the volume of the preimage, which is a solid torus inside the $(n-1)$-sphere.

Hypergeometric functions. The family of *hypergeometric functions* takes $p+q$ parameters and one argument and can be defined as a sum of products of Gamma functions, while the *regularized* version of this function is obtained by dropping the $\Gamma(b_i)$:

$$ {}_pF_q\left(a_1, \ldots, a_p; b_1, \ldots, b_q; z\right) = \sum_{j=0}^{\infty} \left[\prod_{i=1}^{p} \frac{\Gamma(j+a_i)}{\Gamma(a_i)}\right] \left[\prod_{i=1}^{q} \frac{\Gamma(b_i)}{\Gamma(j+b_i)}\right] \frac{z^j}{j!}, \tag{71}$$

$$ {}_p\tilde{F}_q\left(a_1, \ldots, a_p; b_1, \ldots, b_q; z\right) = {}_pF_q\left(a_1, \ldots, a_p; b_1, \ldots, b_q; z\right) / \prod_{i=1}^{q} \Gamma(b_i) \tag{72}$$

$$= \sum_{j=0}^{\infty} \left[\prod_{i=1}^{p} \frac{\Gamma(j+a_i)}{\Gamma(a_i)}\right] \left[\prod_{i=1}^{q} \frac{1}{\Gamma(j+b_i)}\right] \frac{z^j}{j!}. \tag{73}$$

We are interested in the type $p = 3$ and $q = 2$. Here convergence of the infinite sum depends on the values of the parameters. We always have convergence for $z < 1$, and if $z = 1$, then it is necessary to consider the other parameters. A sufficient condition for convergence for $z = 1$ is $b_1 + b_2 > a_1 + a_2 + a_3$ [20].